THE JOURNAL OF PHYSICAL CHEMISTRY C

Article

pubs.acs.org/JPCC

Hysteresis Loop and Scanning Curves for Argon Adsorbed in Mesopore Arrays Composed of Two Cavities and Three Necks

Nikom Klomkliang,[†,‡] D. D. Do,*[,†] and D. Nicholson[†]

[†]School of Chemical Engineering, University of Queensland, ST. Lucia, QLD 4072, Australia

[‡]Chemical Engineering Program and Centre of Excellence for Innovation and Technology for Water Treatment, Faculty of Engineering, Naresuan University, Phitsanulok 65000, Thailand

ABSTRACT: Hysteresis loops and scanning curves for argon adsorbed in sequential mesopore arrays consisting of two cavities and three necks have been studied using Grand Canonical Monte Carlo simulation. We examined four different pore configurations and find that there are two patterns for scanning: (i) Type S1, the scanning curve crosses the hysteresis loop from one boundary to the opposite boundary with the possibility that condensation/evaporation occurs within the hysteresis loop; and (ii) Type S2, the scanning curve leaves one boundary and then returns to the same boundary. The first array has three necks with sizes that are smaller than the critical width (which demarcates cavitation from pore blocking as the mechanism for evaporation from a cavity). The second, third, and fourth arrays are the same as the first with the exception that one neck is larger than the critical width. This large neck connects the large cavity to the gas surroundings in array 2, connects the two cavities in array 3, and connects the small cavity to the gas surroundings in array 4. The mechanism of evaporation from the arrays 1 and 3 is found to be cavitation, they have the same type of hysteresis loop (H2a), but their descending scanning curves (DSC) are different. The DSC of array1 scans across the hysteresis loop (Type S1), while that of array 3 is of Type S2. In arrays 2 and 4, the evaporation follows a sequence of pore blocking and cavitation from the two cavities; a double loop of Type H2a. Although these two arrays have the same type of hysteresis loop, their scanning curves are different. Array 2 has Type S1 scanning with a subloop within the primary hysteresis loop, while array 4 has Type S2 scanning curve with a subloop.

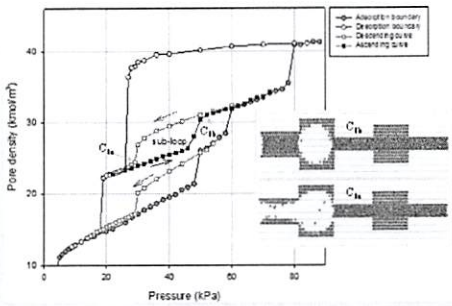

1. INTRODUCTION

Hysteresis associated with capillary condensation and evaporation in mesoporous materials (a range of ~2–50 nm is defined for nitrogen and argon) has been the subject of immense interest for over 100 years[1] because of its use in the characterization of pore size distribution (PSD). The hysteresis loop has been regarded as the fingerprint for the determination of PSD of a given solid, and the connectivity between pores of different sizes could be determined from the analysis of the adsorption–desorption boundaries as suggested by Seaton and others.[2−10] However, it is known that at a given temperature solids with different pore structures can exhibit similar hysteresis loops[11,12] and that their shapes can change significantly with temperature.[13−16] In order to probe pore structure more effectively, additional information needs to be sought, and to this end scanning across the hysteresis loop is proposed as a means of gaining further insight into the structure of the pore array that cannot be deduced from either the adsorption boundary or the desorption boundary of the hysteresis loop.[17−23] Figure 1a shows a desorption scanning curve (DSC) when the pressure is decreased from any point on the adsorption boundary of the hysteresis loop, and an ascending scanning curve (ASC) starting from any point on the desorption boundary when pressure is increased. The subloop of the scanning curve within the hysteresis loop could occur when the pressure is reversed before the scanning curve reaches the opposite boundary. This is the case where there is internal condensation/evaporation, occurring in some regions of the pore array (Figure 1b), and when there is no internal condensation/evaporation the scanning curve is reversible.[24]

An early model referred to in the literature as the independent domain theory of sorption hysteresis[25] can account for many experimental hysteresis loops. The main idea of this theory is that each pore space can fill and empty, independent of the state of its neighbors. Accordingly, desorption and adsorption scanning curves should cross between the adsorption and desorption boundaries. However, experimental scanning curves do not always follow this behavior and can be classified into three broad categories: (i) crossing between the boundary curves of the hysteresis loop with or without internal condensation/evaporation within the hysteresis loop; (ii) returning back to the same boundary; and (iii) intermediate between (i) and (ii), in which the scanning curve converges to the closure point.[17−19,21,22,26−28] Special techniques were also developed to take into account large scale disorders in molecular simulation to study scanning curves.[29,30]

Received: February 4, 2015
Revised: March 19, 2015
Published: April 7, 2015

 © 2015 American Chemical Society

DOI: 10.1021/acs.jpcc.5b01184
J. Phys. Chem. C 2015, 119, 9355−9363

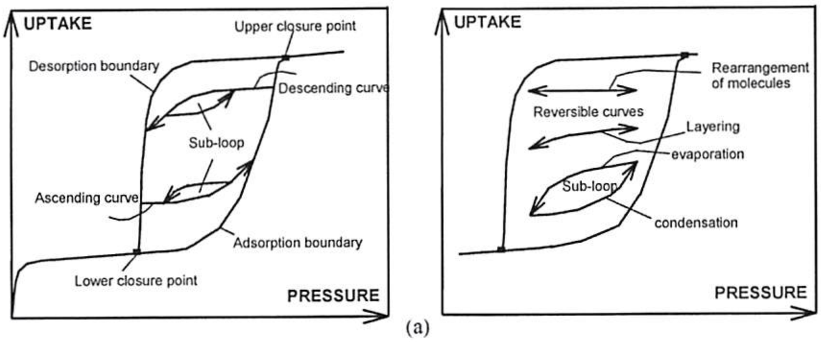

Figure 1. Schematic diagram of (a) scanning curves and (b) subloop within the hysteresis of adsorption isotherm.

Table 1. Four Different Pore Arrays Used in This Work[a]

Pore Array	Schematic diagram	Scanning behavior
1	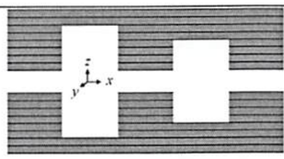	Curves of Type *S1* without evaporation/condensation along the scanning curves. Thus, reversible scanning curves are found.
2	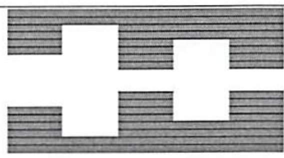	Curves of Type *S1* with evaporation/condensation along the scanning curves. There is therefore a sub-loop within the boundary hysteresis loop.
3	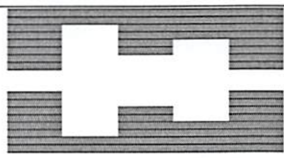	Curves of Type *S2* without any sub-loop within the boundary hysteresis loop.
4	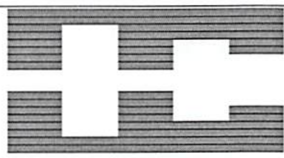	Curves of Type *S2* with sub-loops within the boundary hysteresis loop.

[a]Pore lengths of each section are 6 nm, and the widths of the large cavity, small cavity, large neck, and small neck are 5.82, 4.48, 3.14, and 2 nm, respectively.

Further insight is needed into the microscopic origin of these categories.

In a recent study,[24] we explored the effects of temperature on the scanning of argon adsorption in a wedge pore with either its narrow end or its wide end closed, in order to understand the way in which such a simple connectivity (in the form of a linear variation in the pore size along the axial direction) affects the scanning behavior. In this article, we extend our investigation to more complex systems composed of linear sequential arrays of two cavities and three necks, as examples of networks with the lowest order of connectivity, and use grand canonical Monte Carlo (GCMC) simulation of argon adsorption to study their scanning behavior.

2. THEORY

2.1. Fluid–Fluid Potential Model. We used the Lennard-Jones (LJ) 12–6 equation to calculate the fluid–fluid potential energy of argon, with the following molecular parameters: ε/k_B = 119.8 K and σ = 0.3405 nm.

2.2. Fluid–Solid Potential Model. Arrays of mesopores, with planar graphitic walls, connected to gas reservoirs via necks are shown in Table 1. We used the Bojan–Steele equation[31−33] to calculate the fluid–solid potential energy with a 0.3354 nm spacing between two adjacent graphene layers, which are finite in the x-direction (along the axial direction) and infinite in the y-direction (perpendicular to the page). These arrays have two cavities joined together by a smaller neck, and they are connected to the gas surrounding via two small necks. Depending on the relative sizes of these sections (cavity and neck) and whether the necks are either smaller or larger, the critical width, H_c, demarcates the mode of evaporation in the cavity. If the necks connecting the cavity to the gas surrounding are smaller than H_c, the mechanism of

DOI: 10.1021/acs.jpcc.5b01184
J. Phys. Chem. C 2015, 119, 9355–9363

evaporation of adsorbate in the cavity is cavitation. However, if one of them is greater than H_c, pore blocking is the mechanism.

We studied four different pore arrays, which may give rise to the types of scanning curve listed in Table 1. In the first, all three necks are smaller than the critical width. The second, third, and fourth arrays are the same as the first with the exception that one neck is larger than the critical width. This large neck connects the large cavity to the gas surroundings in array 2, connects the two cavities in array 3, and connects the small cavity to the gas surrounding in array 4.

2.3. Grand Canonical Monte Carlo (GCMC) simulation.

Our GCMC simulation of argon adsorption employs the Metropolis algorithm[34] with equal probabilities of displacement, insertion, and deletion trials. A length of 1×10^8 configurations was used in both equilibration and sampling stages.

The average absolute pore density ($\rho_{\text{pore}}^{\text{ABS}}$) is defined by

$$\rho_{\text{pore}}^{\text{ABS}} = \frac{\langle N \rangle}{V_{\text{acc}}} \tag{1}$$

where $\langle N \rangle$ is the ensemble average of number of particles in the pore and V_{acc} is the accessible pore volume.[35]

The simulation box was divided into slices in the x-direction to calculate the 1-D density distribution, which is given by

$$\rho(x) = \frac{\langle N_{\Delta x} \rangle}{\Delta x H_{\text{acc}} L_y} \tag{2}$$

where $\langle N_{\Delta x} \rangle$ is the average number of molecules in the segment bounded by $(x - \Delta x/2, x + \Delta x/2)$, H_{acc} is the accessible width at a given x, and L_y is the length in the y-direction.

3. RESULTS AND DISCUSSION

3.1. Pore Array 1.

The three necks of array 1 are smaller than the critical width H_c, and therefore, the adsorption and desorption isotherm and corresponding scanning curve are the simplest dealt with in this article. Without loss of generality we shall assume that the three necks are equal in size. The argon isotherms at 87 K together with snapshots of the adsorbate at various points along the adsorption and desorption, which highlight the mechanisms of adsorption and desorption, are shown in Figure 2. Our first observation is that the hysteresis loop is of Type H2a, which is always found when a cavity is connected to the gas surroundings by necks whose sizes are smaller than the critical width. (The critical width H_c is the width of a neck that demarcates the mechanism of evaporation in a cavity connected to the gas surroundings via that neck. If the width of the neck is smaller than H_c the evaporation is by the cavitation, and if it is greater than H_c the evaporation follows the pore blocking mechanism.) This is also the case for array 3 (see below), and this means that two different arrays (with different distributions of section width) can give the same type of hysteresis loop. This raises the question of whether there is a way that adsorption data can discriminate between these two pore configurations. A possible answer can be sought by investigating the scanning curves across the hysteresis loop. We shall first study the scanning curves of array 1 and then consider those of array 3 in section 3.3, where we shall highlight the distinctions between the scanning curves for these two arrays.

3.1.1. Adsorption.

The adsorption mechanism for this type of structure is well-known, but for the sake of completeness we shall briefly describe it here. As pressure is increased from an empty pore, molecular layering occurs on the pore walls, and the thickness of the adsorbed layer increases with pressure up to Point A_1, which is the condensation pressure of the three necks (equal in size). At this point the necks are filled with adsorbate (Point A_2), and it is worth noting that this condensation is that of open ended pores. As pressure is further increased from Point A_2 the adsorbed layers in the two cavities become thicker, and at Point A_3–A_4 condensation occurs in the small cavity, followed by a further increase in the thickness of the adsorbed layer in the large cavity, and finally condensation occurs in this cavity at Point A_5–A_6. Although the adsorption isotherm for this model shows a sequence of three condensation steps associated with the necks, the small cavity and the large cavity; real porous materials would show a smoother increase in the pore density along the adsorption isotherm because they would comprise a larger number of necks and cavities with a distribution in sizes. It should be noted as worthwhile to make a note that if the sizes of all the necks in an extended array are smaller than the critical width, then the type of hysteresis loop and its scanning curves will be similar to those presented for Array 1. The sharp evaporation due to cavitation characterizes the resulting hysteresis loop as a typical H2a Type, according to the new IUPAC classification (in the new IUPAC classification, the old Type H2 becomes Type H2a, and the Type C of de Boer classification was not accounted for in the IUPAC classification).[36]

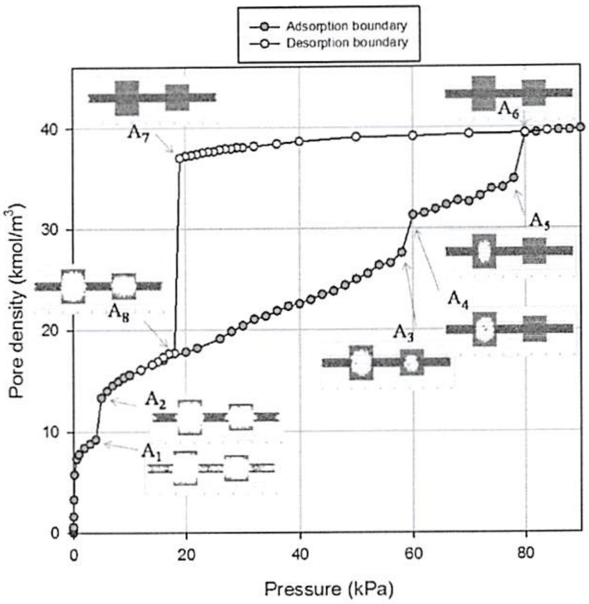

Figure 2. Adsorption–desorption isotherms of argon at 87 K in the pore array 1.

3.1.2. Desorption.

On desorption from a completely filled pore (see Figure 2), the condensed fluid in the two cavities is stretched to Point A_7, at which evaporation from the two cavities occurs via the cavitation mechanism. To support our argument of stretching and cavitation of the adsorbate in the two cavities, we show in Figure 3, the local density distribution along the axial direction of the pore. A small decrease in the density profile from Points A_6 to A_7 can be attributed to the reduction in density due to the stretching of the adsorbate, and at Point A_7 the densities in the two cavities are low enough that the average distance between neighboring molecules can no

DOI: 10.1021/acs.jpcc.5b01184
J. Phys. Chem. C 2015, 119, 9355–9363

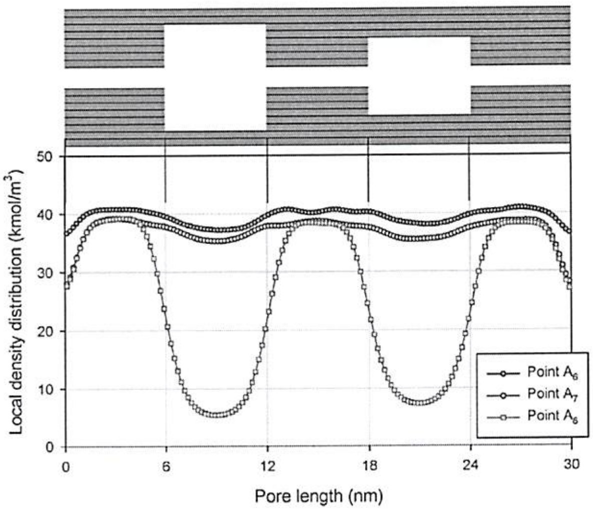

Figure 3. Local density distribution along the pore length of argon at 87 K in pore array 1. Points A_6–A_8 are shown in Figure 2.

longer support a dense fluid-like structure, and cavitation is induced in the cavities with a decrease in mean density to Point A_8.

3.1.3. *Scanning Curves.* For the isotherms of this array 1 (Figure 2), the descending and ascending scanning curves can be made from the nonvertical segments (vertical segments are those associated with the condensation and evaporation) of the boundaries of the hysteresis loop. Descending scanning curves (DSC) are possible from any point along the segment A_8A_3 and A_4A_5. DSCs from the first segment simply trace reversibly along that segment, for example, Point B_1 in Figure 4a. However, DSCs from any point along the segment A_4A_5 will trace across the hysteresis loop, due simply to condensation in some sections of the pore array (in this case condensation in the small cavity).

Figure 4a shows a DSC from any point on the segment A_4A_5. It traces reversibly along this segment (thinning of adsorbed layers in the large cavity) until it reaches Point A_4, from where it transverses across the hysteresis loop to produce the $A_4A_{4a}A_{4b}$ descending curve. The microscopic behavior of this scanning curve is merely a combination of two processes: (1) continued thinning of the adsorbed layers in the large cavity and (2) stretching of condensed fluid in the small cavity. This picture is supported by the local density distributions at various points along the scanning curve (Figure 4b). At Point A_{4b}, which is the cavitation pressure, the adsorbate in the small cavity evaporates via the cavitation process. This DSC is a classical domain theory (almost) "horizontal" scanning curve (not quite "horizontal"

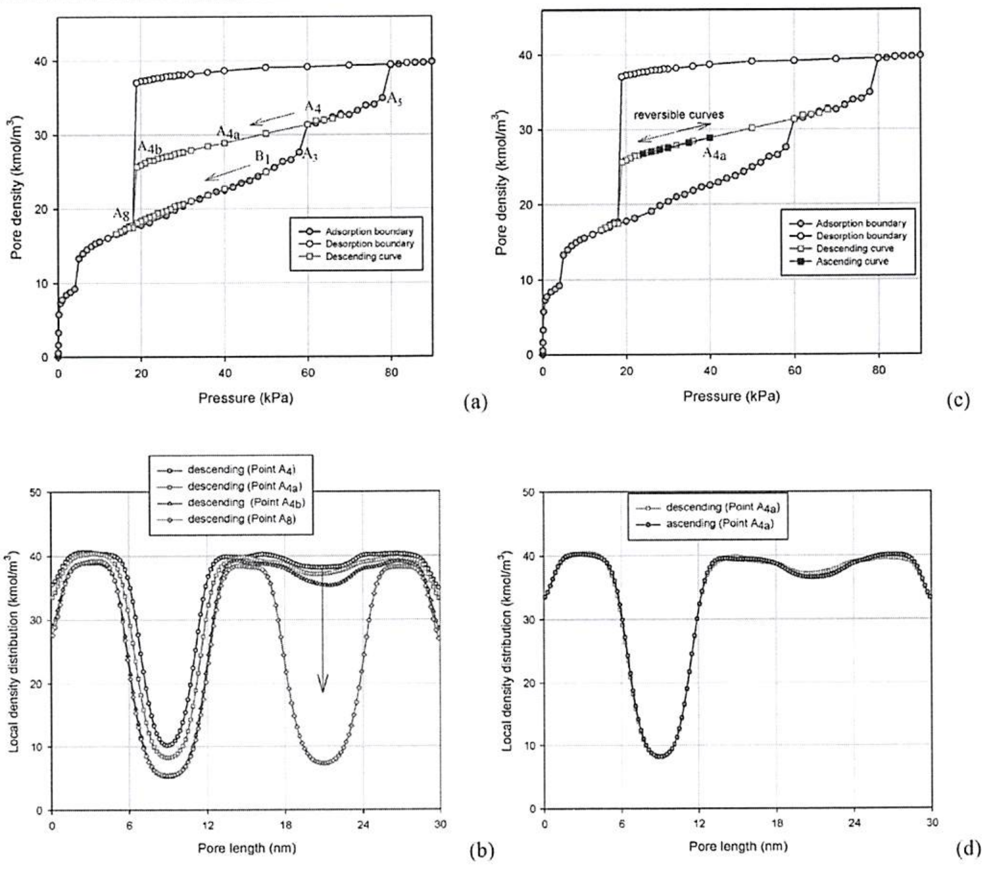

Figure 4. Scanning curves of argon at 87 K in the pore array 1: (a) descending scanning curve, (b) local density distribution of descending scanning curve from Points A_4 to A_8, (c) ascending scanning curve, and (d) local density distribution of descending and ascending scanning curves at Point A_{4a}.

DOI: 10.1021/acs.jpcc.5b01184
J. Phys. Chem. C 2015, 119, 9355–9363

because of the thinning of the adsorbed layer in the large cavity and the stretching of adsorbate in the small cavity), spanning across the hysteresis loop, and since there is no internal condensation or evaporation along the scanning, this scanning curve is reversible. If the DSC scan stops at any points between A_4−A_{4b} and the pressure direction is reversed (i.e., increased) it traces exactly the same path back to Point A_4. To further support the reversibility of this scanning, we show in Figure 4d the local density distributions at Point A_{4a} along the descending and ascending paths (Figure 4c), and they completely overlap with each other.

3.2. Pore Array 2. This array has two necks smaller than the critical width H_c and the neck connecting the large cavity to the gas surroundings greater than H_c. The adsorption and desorption isotherms are shown in Figure 5, and the snapshots

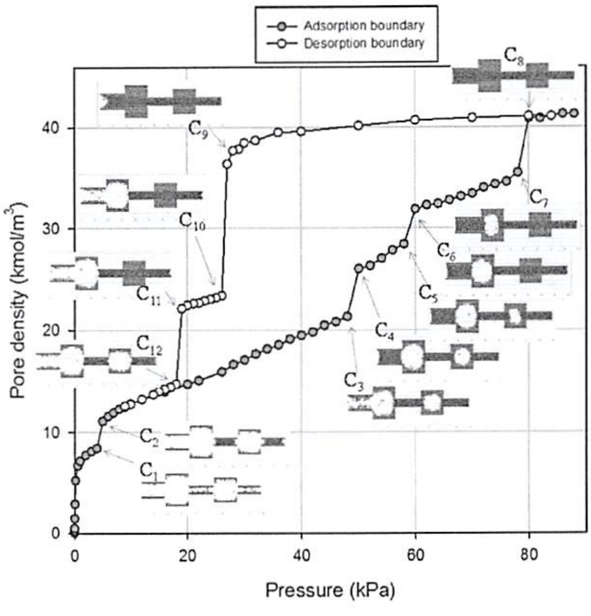

Figure 5. Adsorption−desorption isotherms of argon at 87 K in array 2.

for various points along the boundaries of the hysteresis loop are also included in this figure to show the mechanisms of adsorption and desorption. The hysteresis loop for this array is similar to that of Array 4; a double Type H2a, but as we shall show later, the scanning curves for these two pore arrays are different, supporting the notion that the scanning curves could be used to fine-tune the determination of porous structure.

3.2.1. Adsorption. The mechanism of adsorption is straightforward; the condensation in the two small necks at C_1 to C_2, which is lower than the cavitation pressure, is followed by a sequence of condensations in the three sections of the pore: (1) the large neck at C_3C_4, (2) the small cavity at C_5C_6, and (3) the large cavity at C_7C_8.

3.2.2. Desorption. Along the desorption branch, the adsorbate in the large cavity empties first along the vertical segment C_9C_{10}, via a pore blocking mechanism, because it is connected to the gas surroundings via the large neck whose width is greater than H_c. On further reduction of cavitation of adsorbate takes place in the small cavity at C_{11}, which empties along the segment $C_{11}C_{12}$. To confirm that the mechanism of evaporation from the large cavity is pore blocking we show, in Figure 6, the axial local density distributions at Points C_8, C_9, and C_{10}. These clearly show the recession of the meniscus,

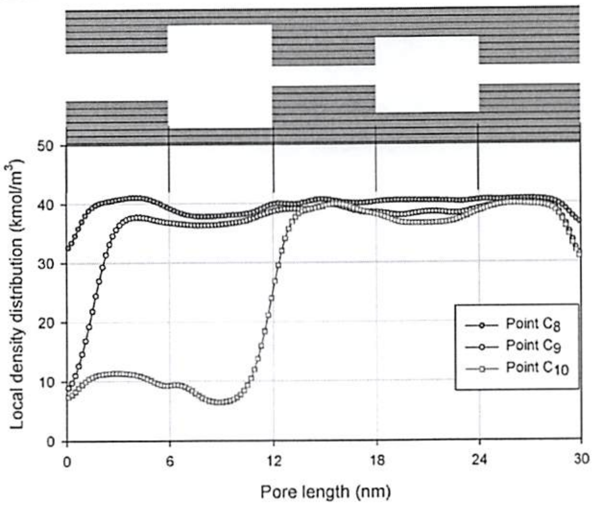

Figure 6. Local axial density distributions in array 2: Points C_8−C_{10} are as located in Figure 5.

formed at the open end of the large neck, into the interior, and the evaporation of adsorbate when it reaches the junction between the neck and the cavity. This is a pore blocking mechanism of evaporation.

3.2.3. Scanning Curves. There are three segments on the adsorption boundary where descending scanning can be made: C_2−C_3, C_4−C_5, and C_6−C_7. DSCs from any point along the first segment trace reversibly, as already discussed for segment A_8−A_3 for the pore Array 1.

Descending scanning from any point along the segment C_6−C_7 reveals interesting behavior because two condensation steps occur before this segment. The descending curve scans this segment reversibly up to Point C_6 and then spans across the hysteresis loop to terminate at Point C_{10} via Point C_{6a}. This path is associated with evaporation from the large neck, which behaves like an open ended pore, and therefore, the evaporation occurs at a slightly higher pressure than the pressure required for the evaporation from this neck and the large cavity when the pore is filled with adsorbate because in the latter case the large neck would behave like a closed end pore.

The ascending scanning curve (ASC) can start at any point in the segment C_{11}−C_{6a} of the desorption boundary, where only the small cavity and the two small necks are full, the ascending curve leaves the desorption boundary at C_{10}, and condensation occurs in the large neck at Point C_{6b} and then reaches the adsorption boundary at Point C_6 as shown in Figure 6b. These ASC and the DSC from Point C_6 form a subloop within the hysteresis loop. This subloop is associated with the evaporation/condensation in the large neck as an open end pore, and this is supported by the axial local density distributions at the subclosure Points C_{6a} and C_{6b} shown in Figure 7c.

Descending from any points on the segment of C_4−C_5 (see Figure 7a) of the adsorption boundary, where the three necks are full and the two cavities are empty except for adsorbed layers on the walls, the desorption curve spans the boundary hysteresis loop with a gradual decrease in density associated

DOI: 10.1021/acs.jpcc.5b01184
J. Phys. Chem. C 2015, 119, 9355−9363

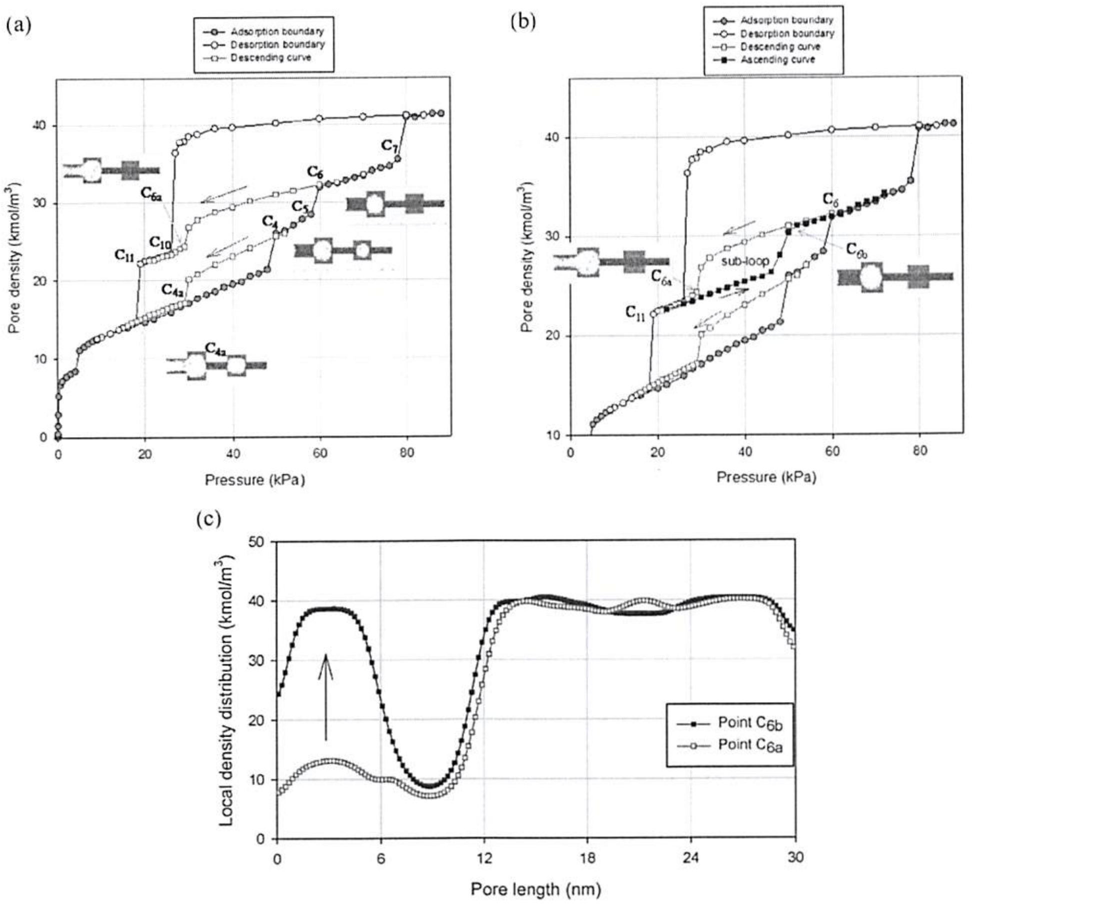

Figure 7. Scanning curves for argon at 87 K in array 2: (a) descending scanning curve, (b) ascending scanning curve, and (c) local density distributions at Points C_{6a} and C_{6b}.

with the thinning of the adsorbed layers in the two cavities and recession of menisci in the large neck (and to a lesser extent in the two small necks). This is then followed by evaporation of adsorbate from the large neck, which behaves like an open end pore, and the scanning curve returns to the adsorption boundary at Point C_{4a}. This phenomenon of returning back to the same boundary has not been previously recognized in the literature and will be encountered again for arrays 3 and 4.

3.3. Pore Array 3.

The cavities in this array are connected to the gas surroundings via two necks with widths smaller than H_c and joined together by a neck larger than H_c. The isotherms and the scanning curves are shown in Figure 8. The type of hysteresis loop for this pore is the same as for array 1; Type H2a. In array 1 we observed that the descending curve spanned the hysteresis loop and joined the desorption boundary at the cavitation stage. However, in array 3 the DCS spans the loop but returns back the adsorption boundary, not at the lower closure point but at a higher pressure. This conclusion is not changed if the numbers and order of cavities and necks are changed; as long as the large necks (greater than the critical width) connect between cavities and smaller necks (smaller than the critical width) connect the cavities to the surroundings, the hysteresis type will be Type H2a and the scanning curve will be Type S2 as we have found for array 3.

3.3.1. *Adsorption and Desorption.*

The adsorption mechanism follows a sequence of four condensation steps:

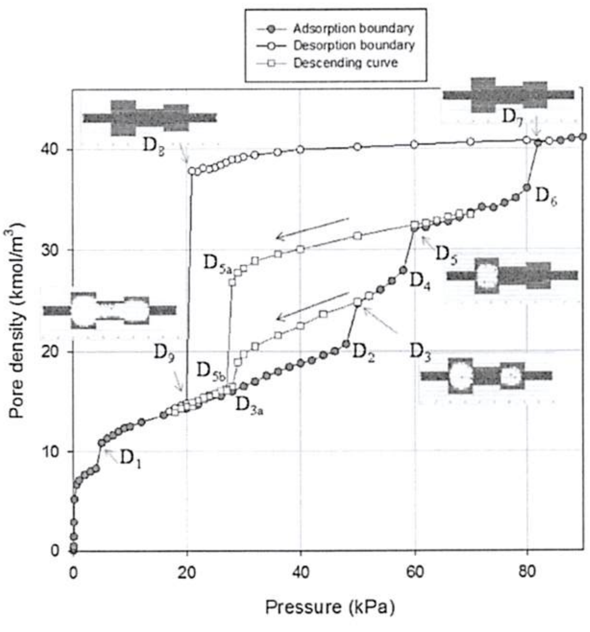

Figure 8. Adsorption−desorption isotherms and descending scanning curve of argon at 87 K in array 3.

DOI: 10.1021/acs.jpcc.5b01184
J. Phys. Chem. C 2015, 119, 9355−9363

(1) the two small necks, (2) the large neck, (3) the small cavity, and (4) the large cavity, and desorption proceeded by cavitation from the two cavities and the large neck at Points D_8–D_9.

3.3.2. Scanning Curve. The descending scan can be made from any point on the segments D_3–D_4 and D_5–D_6. For any point on the segment D_5–D_6, the pore except for the large cavity, is filled with adsorbate; the descending scanning curve is reversible in this segment until Point D_5 is reached. When pressure is reduced further, the curve spans across the hysteresis loop to reach Point D_{5a}, where the large neck evaporates like a closed end pore by recession of the meniscus and instant evaporation from the small cavity (pore blocking mechanism) to Point D_{5b}. This mechanism is confirmed by the snapshots and the local density distributions shown in Figure 9.

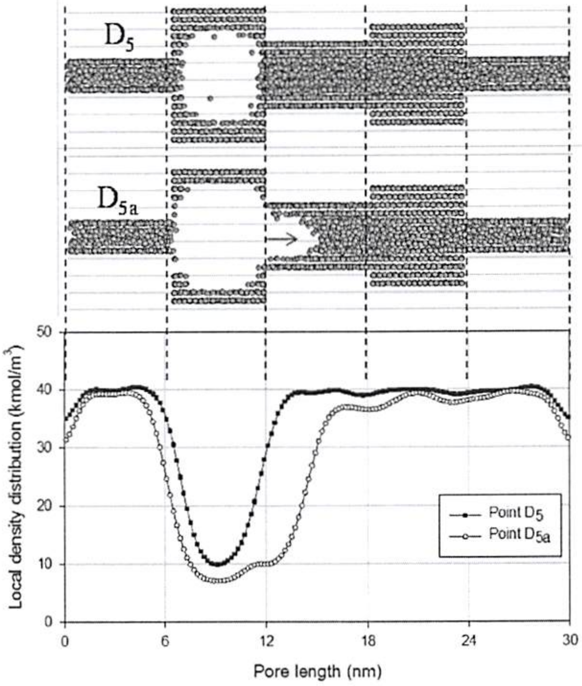

Figure 9. Local density distribution and snapshots in array 3. Points D_5 and D_{5a} are shown in Figure 8.

It is important to note here that this evaporation at D_{5b} is at a higher pressure than the cavitation pressure encountered for desorption from a completely filled pore. Thus, the scanning curve does not join the lower closure point.

The other path for descending scan starts from the segment D_3–D_4. The scanning curve traces this segment to Point D_3, where the two cavities are not full and the large neck behaves like an open end pore; therefore, the DSC scans across the hysteresis loop and evaporation from the large neck occurs at Point D_{3a}. Since this point corresponds to evaporation from an open end-like large neck, its evaporation pressure is greater than the evaporation pressure from the large neck at Point D_{5b}, where the large neck behaves like a closed end pore.

3.4. Pore Array 4. In this array, two necks are smaller than H_c and the other neck, which connects the small cavity to the gas surroundings, is larger than H_c. The isotherms and scanning curves are shown in Figures 10 and 11, respectively. The

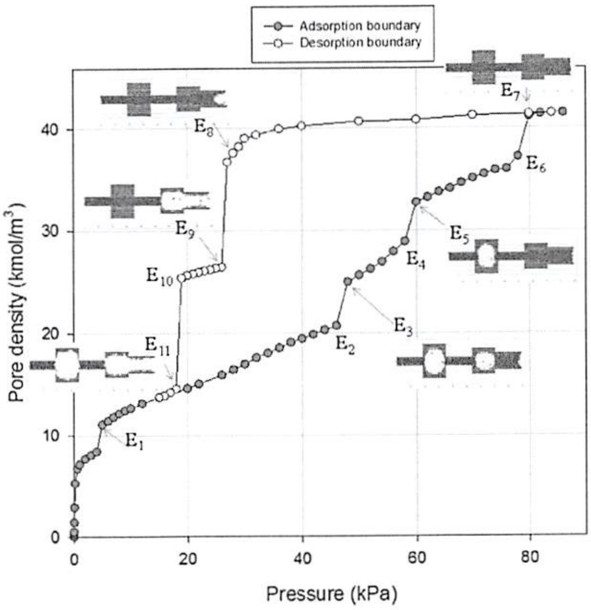

Figure 10. Adsorption–desorption isotherms of argon at 87 K in the pore array 4.

boundary hysteresis loop for this array is the same as that for array 2, but the scanning curves of array 2 cross the hysteresis loop, connecting the desorption and adsorption boundaries exception of the lower DSC, while the scanning curves for array 4 (descending and ascending) leave the boundary (adsorption and desorption) and then return to the same boundary, at a pressure above the closure point.

3.4.1. Adsorption and Desorption. The adsorption mechanism in this array is similar to that for arrays 2 and 3, with a sequence of four condensation steps: (1) small necks, (2) large neck, (3) small cavity, and (4) large cavity. The order of condensation in the two cavities is a small cavity followed by large cavity. Desorption occurs by evaporation from the small cavity first via pore blocking, followed by evaporation from the large cavity at a lower pressure, via the cavitation mechanism. This sequence is followed because the small cavity is connected to the gas surroundings by the larger neck. It is this feature of evaporation from the smaller cavity first that makes the behavior of scanning in this array richer than the other arrays discussed so far.

3.4.2. Scanning Curves. There are two segments along the adsorption boundary from which a descending scan can be made: E_3–E_4 and E_5–E_6. We present in Figure 11a the scanning curve from a point on the segment E_3–E_4 where two cavities are empty except for adsorbed layers on the walls. The DSC leaves this segment at Point E_3, and the scan spans the loop as the menisci recede in the large neck; adsorbate then evaporates from this neck as an open end pore. Therefore, the evaporation pressure is slightly greater than the evaporation pressure at Point E_9 where the large neck behaves like a closed end pore. The descending scan from a point on the segment E_5–E_6 is associated with evaporation from the small cavity via pore blocking of the large neck. This evaporation pressure for the large neck, behaving like a closed end pore, is slightly lower than when the DSC starts from any point along the segment E_3–E_4 and is the same as the first evaporation pressure along the desorption boundary.

DOI: 10.1021/acs.jpcc.5b01184
J. Phys. Chem. C 2015, 119, 9355–9363

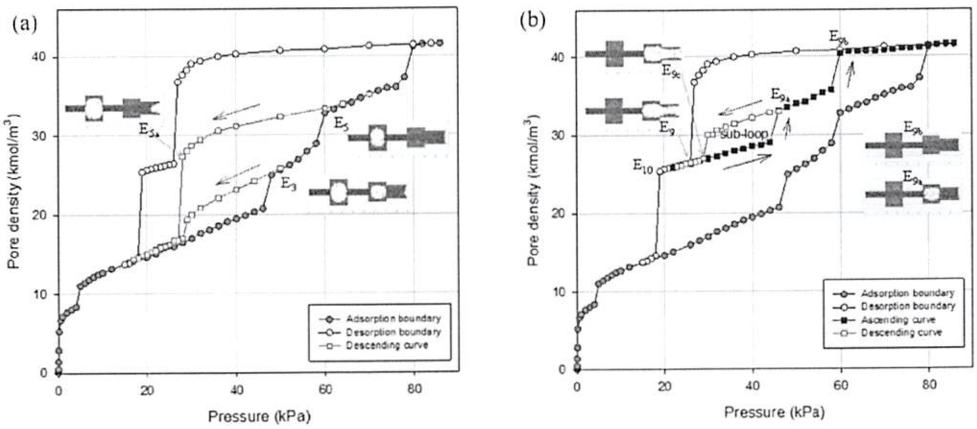

Figure 11. Scanning curves of argon at 87 K in array 4: (a) descending scanning curve and (b) ascending scanning curve.

Figure 11b shows the ascending curve from any point on the segment E_9-E_{10} where only the large cavity and the two small necks are filled with adsorbate. The ASC spans the loop and is associated with the layering and then condensation in the large neck, behaving as an open end pore, at Point E_{9a}, followed by the condensation in the small cavity at Point E_{9b} as pressure is further increased. It is interesting that in this ascending scanning curve we note that the large cavity is filled first, followed by the small cavity; in contrast to the adsorption boundary where the small cavity is filled first followed by the large cavity. Once the ascending scanning curve has reached Point E_{9a} the pressure is reversed (i.e., decrease in pressure), the subdescending scanning curve is then associated with the evaporation from the open end-like large neck, resulting in a subloop within the main hysteresis loop. Thus, the subloop could be regarded as the condensation/evaporation for the large neck, falling between the condensations in the two cavities. This is exactly the case that we observed earlier for array 2.

4. CONCLUSIONS

We have used GCMC simulation to investigate the hysteresis loop and its scanning curves in pore arrays consisting of two cavities and three necks. Depending on the relative sizes of the cavities and the necks, there are four sequential pore arrays that give a distinct behavior for the scanning curves. The first array has all three necks smaller than the critical width, H_c. The second, third, and fourth arrays are the same as the first except that one neck is larger than H_c, and this large neck connects the large cavity to the gas surroundings in array 2, connects the two cavities in array 3, and connects the small cavity to the gas surroundings in array 4.

It is found that the type of hysteresis obtained for arrays 1 and 3 are the same (Type H2a) with cavitation as the sole mechanism for evaporation. There is no subloop in these arrays. However, the descending curve of array 1 is of Type S1 (crossing between the main boundaries), while Type S2 (returning back to the same boundary) is found for array 3.

Pores 2 and 4 exhibit a double Type H2a hysteresis loop in which pore blocking controls the first stage of evaporation, and cavitation is the mechanism in the second stage. However, the scanning curves of the array 2 are of Type S1, but its behavior is different from that of array 1, in that there is a subloop, resulting from the internal evaporation/condensation within the main hysteresis loop. However, the scanning curves of the array 4 span within the hysteresis loop via layering and internal evaporation/condensation (which can reproduce a subloop within the hysteresis loop), before turning back onto the same boundary (Type S2).

Our proposed pore model with two cavities and three necks provides the simplest example of a network (with connectivity 2) that produces a rich behavior in the hysteresis loop and its scanning curves, both descending and ascending.

■ AUTHOR INFORMATION

Corresponding Author

*E-mail: d.d.do@uq.edu.au.

Notes

The authors declare no competing financial interest.

■ ACKNOWLEDGMENTS

This work is supported by the Australian Research Council. The authors also acknowledge the support from the Thailand Research Fund (Contract TRG5780126).

■ REFERENCES

(1) Horikawa, T.; Do, D. D.; Nicholson, D. Capillary Condensation of Adsorbates in Porous Materials. *Adv. Colloid Interface* **2011**, *169*, 40−58.

(2) Brunauer, S.; Mikhail, R. S.; Bodor, E. E. Pore Structure Analysis without a Pore Shape Model. *J. Colloid Interface Sci.* **1967**, *24*, 451−463.

(3) Brunauer, S.; Mikhail, R. S.; Bodor, E. E. Some Remarks about Capillary Condensation and Pore Structure Analysis. *J. Colloid Interface Sci.* **1967**, *25*, 353−358.

(4) Mikhail, R. S.; Brunauer, S.; Bodor, E. E. Investigations of a Complete Pore Structure Analysis: II. Analysis of Four Silica Gels. *J. Colloid Interface Sci.* **1968**, *26*, 54−61.

(5) Mason, G. The Effect of Pore Space Connectivity on the Hysteresis of Capillary Condensation in Adsorption—Desorption Isotherms. *J. Colloid Interface Sci.* **1982**, *88*, 36−46.

(6) Seaton, N. A. Determination of the Connectivity of Porous Solids from Nitrogen Sorption Measurements. *Chem. Eng. Sci.* **1991**, *46*, 1895−1909.

(7) Liu, H.; Zhang, L.; Seaton, N. A. Determination of the Connectivity of Porous Solids from Nitrogen Sorption Measurements. II. Generalisation. *Chem. Eng. Sci.* **1992**, *47*, 4393−4404.

(8) Liu, H.; Zhang, L.; Seaton, N. A. Sorption Hysteresis as a Probe of Pore Structure. *Langmuir* **1993**, *9*, 2576−2582.

DOI: 10.1021/acs.jpcc.5b01184
J. Phys. Chem. C 2015, 119, 9355−9363

(9) Liu, H.; Seaton, N. A. Determination of the Connectivity of Porous Solids from Nitrogen Sorption Measurements. III. Solids Containing Large Mesopores. *Chem. Eng. Sci.* **1994**, *49*, 1869–1878.

(10) Nicholson, D. Capillary Models for Porous Media. Part 2. Sorption Desorption Hysteresis in Three Dimensional Networks. *Trans. Faraday Soc.* **1968**, *64*, 3416–3424.

(11) Fan, C.; Do, D. D.; Nicholson, D. Condensation and Evaporation in Capillaries with Nonuniform Cross Sections. *Ind. Eng. Chem. Res.* **2013**, *52*, 14304–14314.

(12) Nguyen, P. T. M.; Do, D. D.; Nicholson, D. Pore Connectivity and Hysteresis in Gas Adsorption: A Simple Three-Pore Model. *Colloids Surf., A* **2013**, *437*, 56–68.

(13) Reichenbach, C.; Kalies, G.; Enke, D.; Klank, D. Cavitation and Pore Blocking in Nanoporous Glasses. *Langmuir* **2011**, *27*, 10699–10704.

(14) Morishige, K. Adsorption Hysteresis in Ordered Mesoporous Silicas. *Adsorption* **2008**, *14*, 157–163.

(15) Ravikovitch, P. I.; Neimark, A. V. Experimental Confirmation of Different Mechanisms of Evaporation from Ink-Bottle Type Pores: Equilibrium, Pore Blocking, and Cavitation. *Langmuir* **2002**, *18*, 9830–9837.

(16) Klomkliang, N.; Do, D. D.; Nicholson, D. Effects of Temperature, Pore Dimensions and Adsorbate on the Transition from Pore Blocking to Cavitation in an Ink-Bottle Pore. *Chem. Eng. J.* **2014**, *239*, 274–283.

(17) Cychosz, K. A.; Guo, X.; Fan, W.; Cimino, R.; Gor, G. Y.; Tsapatsis, M.; Neimark, A. V.; Thommes, M. Characterization of the Pore Structure of Three-Dimensionally Ordered Mesoporous Carbons Using High Resolution Gas Sorption. *Langmuir* **2012**, *28*, 12647–12654.

(18) Rasmussen, C. J.; Vishnyakov, A.; Thommes, M.; Smarsly, B. M.; Kleitz, F.; Neimark, A. V. Cavitation in Metastable Liquid Nitrogen Confined to Nanoscale Pores. *Langmuir* **2010**, *26*, 10147–10157.

(19) Monson, P. A. Understanding Adsorption/Desorption Hysteresis for Fluids in Mesoporous Materials Using Simple Molecular Models and Classical Density Functional Theory. *Microporous Mesoporous Mater.* **2012**, *160*, 47–66.

(20) Grosman, A.; Ortega, C. Influence of Elastic Deformation of Porous Materials in Adsorption-Desorption Process: A Thermodynamic Approach. *Phys. Rev. B* **2008**, *78*, 085433.

(21) Cimino, R.; Cychosz, K. A.; Thommes, M.; Neimark, A. V. Experimental and Theoretical Studies of Scanning Adsorption–Desorption Isotherms. *Colloids Surf., A* **2013**, *437*, 76–89.

(22) Esparza, J. M.; Ojeda, M. L.; Campero, A.; Dominguez, A.; Kornhauser, I.; Rojas, F.; Vidales, A. M.; Lopez, R. H.; Zgrablich, G. N_2 Sorption Scanning Behavior of SBA-15 Porous Substrates. *Colloids Surf., A* **2004**, *241*, 35–45.

(23) Coasne, B.; Gubbins, K. E.; Pellenq, R. J. M. Domain Theory for Capillary Condensation Hysteresis. *Phys. Rev. B* **2005**, *72*, 024304.

(24) Klomkliang, N.; Do, D. D.; Nicholson, D. Hysteresis Loop and Scanning Curves of Argon Adsorption in Closed-End Wedge Pores. *Langmuir* **2014**, *30*, 12879–12887.

(25) Everett, D. H.; Smith, F. W. A General Approach to Hysteresis. Part 2: Development of the Domain Theory. *Trans. Faraday Soc.* **1954**, *50*, 187–197.

(26) Tompsett, G. A.; Krogh, L.; Griffin, D. W.; Conner, W. C. Hysteresis and Scanning Behavior of Mesoporous Molecular Sieves. *Langmuir* **2005**, *21*, 8214–8225.

(27) Morishige, K. Hysteresis Critical Point of Nitrogen in Porous Glass: Occurrence of Sample Spanning Transition in Capillary Condensation. *Langmuir* **2009**, *25*, 6221–6226.

(28) Hitchcock, I.; Lunel, M.; Bakalis, S.; Fletcher, R. S.; Holt, E. M.; Rigby, S. P. Improving Sensitivity and Accuracy of Pore Structural Characterisation Using Scanning Curves in Integrated Gas Sorption and Mercury Porosimetry Experiments. *J. Colloid Interface Sci.* **2014**, *417*, 88–99.

(29) Puibasset, J. Adsorption/Desorption Hysteresis of Simple Fluids Confined in Realistic Heterogeneous Silica Mesopores of Micrometric Length: A New Analysis Exploiting a Multiscale Monte Carlo Approach. *J. Chem. Phys.* **2007**, *127*, 154701.

(30) Puibasset, J. Monte-Carlo Multiscale Simulation Study of Argon Adsorption/Desorption Hysteresis in Mesoporous Heterogeneous Tubular Pores like MCM-41 or Oxidized Porous Silicon. *Langmuir* **2009**, *25*, 903–911.

(31) Bojan, M. J.; Steele, W. A. Computer Simulation of Physisorption on a Heterogeneous Surface. *Surf. Sci.* **1988**, *199*, L395–L402.

(32) Bojan, M. J.; Steele, W. A. Computer-Simulation of Physisorption Kr on a Heterogeneous Surface. *Langmuir* **1989**, *5*, 625–633.

(33) Bojan, M. J.; Steele, W. A. Computer-Simulation of Physical Adsorption on Stepped Surfaces. *Langmuir* **1993**, *9*, 2569–2575.

(34) Allen, M. P.; Tildesley, T. P. *Computer Simulation of Liquids*; Clarendon: Oxford, U.K., 1987.

(35) Do, D. D.; Herrera, L. F.; Do, H. D. A New Method to Determine Pore Size and Its Volume Distribution of Porous Solids Having Known Atomistic Configuration. *J. Colloid Interface Sci.* **2008**, *328*, 110–119.

(36) Thommes, M.; Cychosz, K. Physical Adsorption Characterization of Nanoporous Materials: Progress and Challenges. *Adsorption* **2014**, *20*, 233–250.

DOI: 10.1021/acs.jpcc.5b01184
J. Phys. Chem. C 2015, 119, 9355–9363